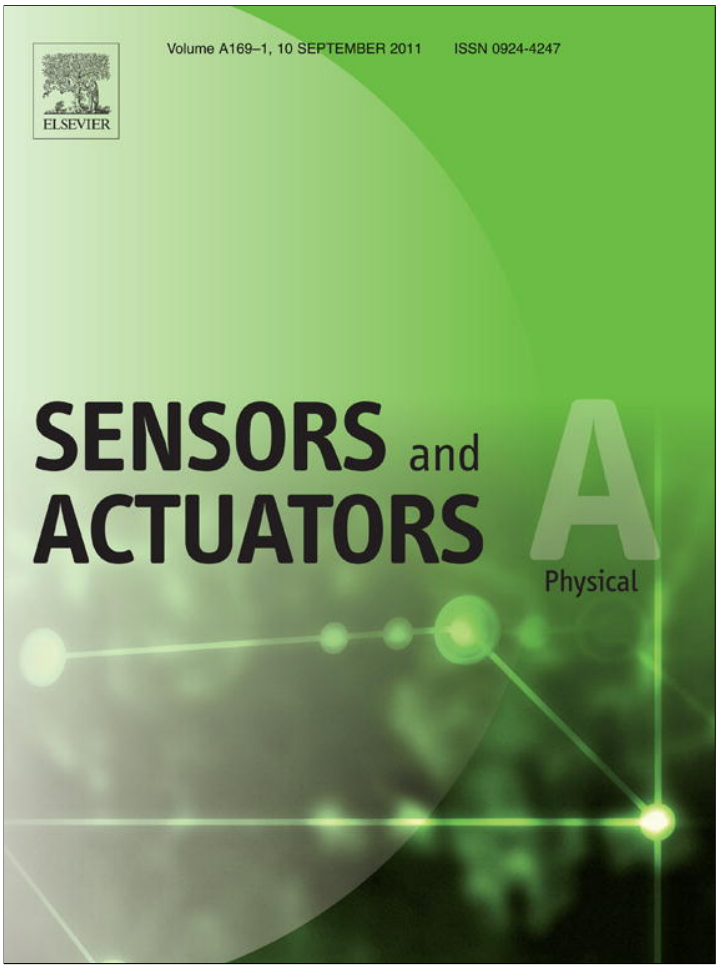

Sensors and Actuators A 169 (2011) 194–205

Contents lists available at ScienceDirect

Sensors and Actuators A: Physical

journal homepage: www.elsevier.com/locate/sna

A new bubble-driven pulse pressure actuator for micromixing enhancement

B. Wang[a], J.L. Xu[a,*], W. Zhang[a], Y.X. Li[b]

[a] Beijing Key Laboratory of New and Renewable Energy, North China Electric Power University, Beijing 102206, PR China
[b] Micro Energy System Laboratory, Guangzhou Institute of Energy Conversion, Chinese Academy of Science, Guangzhou 510640, PR China

ARTICLE INFO

Article history:
Received 21 December 2010
Received in revised form 13 May 2011
Accepted 13 May 2011
Available online 23 May 2011

Keywords:
Thermal bubble
Pulse heating
Actuator
Micromixing
Mixing degree

ABSTRACT

We demonstrate a thermal bubble-driven loop actuator for microfluidic applications. The working principle is similar to that of human being's heart. The actuator consists of a diverging section and a circular chamber. A slim microheater was deposited on the back surface of the glass cover, facing the diverging section of the bottom substrate. The Marangoni effect switches the states of a "long" bubble during the pulse duration stage and a sphere or a circular bubble during the pulse off stage, exporting the pulse pressure and yielding a large convection heat transfer at the vapor–liquid interface. Besides, the loop configuration pumps the bulk fluid movement around the loop. The above features protect the microheater from burnout and dissipate the Joule heat generated by the pulse heating to the supporting structure of the chip substrate, keeping the chip at the room temperature level. The newly designed loop actuator can be integrated with microfluidic systems. The loop actuator has no moving parts thus it has high reliability. Because the thermal bubble never comes out of the loop actuator, the actuator is attractive for biology applications. We demonstrate the loop actuator used for mixing enhancement. The low pulse frequency such as 10 Hz yields a wavy mixing interface, but the high pulse frequencies result in a set of mixing clouds in the mixing channel. The mixing degrees are increased with increases in pulse frequencies. The fluid samples are uniformly distributed across the channel width direction for the pulse frequency of 100 Hz. The mixing degree can reach 0.94 for a short mixing length of about a couple of millimeter at the pulse frequency of 100 Hz. The fluid Reynolds number does not influence the mixing degrees in the mixing channel.

1. Introduction

Mixing two fluids are now widely used in biology and biotechnology. Applications include analysis of DNA and proteins, high throughput screening, chemical reactions, and transfer of small volume of fluids (1–100 nl) of materials. Efficient, simple, and reliable microfluidic devices are attractive to handle the mixing process of two fluids [1]. Commonly, microfluidic devices with the cross sectional dimension of l–100 μm are characterized by low values of Reynolds number. Strategies for controlling flow in microchannels should not depend on the inertia effects, because these are only important for $Re \gg 1$. In other words, mixing two fluids only depends on the molecular diffusion for the laminar flow at low Reynolds number. The diffusive mixing is slow compared with the convection of material along the channel. For the uniaxial flows, the distance along the channel that is required for mixing to occur is very long (≫1 cm) and grows linearly with the Peclet number (*Pe*) [1].

In order to enhance the mixing in microchannels, special mechanisms must be used to manipulate fluids to increase the interfacial surface area, allowing the diffusion be completed in a short time [2]. Various research groups have developed micromixers using moving parts for generating vortex flow or varying pressure gradient, which are called active micromixers. Ultrasonic [3], magnetic microstirrer [4], and bubble-induced acoustic mixing [5] are examples of active micromixers, requiring the use of external energy. Because of their relatively high cost of the hardware components, they are often not suitable for disposal systems. However, the advantage of the active micromixers is that they can provide an excellent mixing performance in a short time. On the other hand, micromixer using no energy input except the fluid driving mechanism (pressure head or pump) is called passive micromixer, having the advantages of no complex control units, no additional input energy, and low fabrication cost.

Various methods using pressure and/or flow filed perturbation are proposed to promote the mixing in low Reynolds number region. Glasgow and Aubry [6] analyzed the effect of the pulsating flow rate in one inlet as well as in the two inlets, and demonstrate that the best results occur when both inlets are pulsed out of phase. In that case, the interface is shown to stretch, retain one fold, and sweep through the confluence zone, leading to good

* Corresponding author.
E-mail address: xjl@ncepu.edu.cn (J.L. Xu).

0924-4247/$ – see front matter © 2011 Elsevier B.V. All rights reserved.
doi:10.1016/j.sna.2011.05.017

mixing within 2 mm downstream of the confluence, i.e. about 1 s of contact. From a practical viewpoint, the case where the inlets are 180° out of phase is of particular interest as the outflow is constant.

Huang et al. [7] proposed a cross-shaped micromixer featuring a pair barrier within the mixing channel. The proposed device obtains a rapid mixing of two sample fluids by means of the electrokinetic instability-induced shedding effects which are produced when a DC electric filed of an appropriate is applied. The proposed device uses a single high voltage power source to simultaneously drive and mix the sample fluids. The tested mixing performance of 96% at a cross-section located 1 mm downstream of the cross-junction when an electric field of 300 V/cm is applied.

Tabeling et al. [8] concentrated on a particular micromixer that exploits chaotic trajectories to achieve mixing. The micromixer is a cross-channel intersection, in which a main stream is perturbed by an oscillatory flow, driven by an external source. One will obtain wavy and chaotic regions depending on the amplitude and frequency of the oscillatory flow. A spatiotemporal resonance phenomenon, in which the material-line deformation is transient, is shown.

Bubble driven actuator for mixing enhancement in microsystems was reported by Tsai and Lin [9]. The oscillatory flow generated by the micropump can induce wavy interface to increase the contact area of mixing fluids to accelerate the mixing process. The tested channels are 200 μm wide, 50 μm deep and the speed of the mixing liquids are measured at 6.5 μl/min. An optimal actuating frequency was found to be 200 Hz. A gas bubble filter is integrated at the downstream of the mixing system to separate the generated bubble from the mixed fluid samples.

We note that using the pulsating flow to enhance the micromixing is not a new concept. The perturbation source comes from the external fluid source, acoustic actuated perturbation, high DC voltage electrokinetic induced interface instability, etc. The methods to generate the perturbation are too many and they are not described here one by one. Most of them either depend on the complex external or internal hardware, or are not suitable for portable use. The pulsating flow is a good strategy for micromixing, but the key issue is how to generate the pulsating flow with simple hardware and low cost.

In this paper, we report a new thermal bubble-driven loop actuator for microfluidic applications under the situation that the perturbation pressure source is required. The working principle of the actuator is similar to that of a human being or animal's heart. A pulse pressure export can be connected with any microfluidic component, thus it can be used for a common actuator module. We report the actuator used for the mixing enhancement in a Y-shaped microchannel. The pulse pressure export is arranged perpendicular with respect to the mixing channel, generating the transverse flow components in the mixing channel. It is found that the mixing degree can reach 94% for a very short mixing length of 1–2 mm downstream of the pulse pressure export. The mixing performance is easily controlled by the pulse voltage frequency. The dynamic bubble confined in the loop actuator not only does not "heat" the fluid sample in the mixing channel, but also does not block the mixing channel. Because the thermal bubble never reaches the mixing channel, a bubble filter is not necessary along the mixing channel. The external hardware to drive the actuator is just a pulse voltage generator with low amplitude. These features provide the advantages over other pressure perturbation methods reported in the literature previously. Besides, because there are no moving components, the proposed actuator has high reliability.

2. Experiment

2.1. Design of the bubble driven actuator for pulse pressure generation

Thermal bubble-driven actuators are reported previously in the literature for microfluidic applications. To the authors' knowledge, three key issues limited their commercial application in real systems. Firstly, for biology applications, the biology fluid sample directly contacts the bubble. The "heating" effect significantly influences the sample properties. Secondly, even though many studies have been performed for the bubble dynamics on the thin film microheater under the pulse heating condition driven by the ink-jet applications, the topic is still open. For instance, the thin film heater may be burnout under an un-suitable pulse heating parameter. Xu and Zhang [10] reported that there are three types of bubble behaviors over a wide range of pulse heating parameters. The third type, called the bubble size oscillation and large bubble formation, involves an initial explosive boiling, followed by a periodic bubble growth and shrinking. Then the bubble continues to increase its size, until a constant bubble size is reached which is significantly larger than the thin film microheater itself. This situation is dangerous because the thin film heater is always covered by the vapor bubble. The thin liquid film under the vapor bubble may be dryout. Thirdly, for a flowing system, the bubble should be removed out of the system. Thus a bubble filter shall be used, increasing the system complicity.

Here we demonstrate the newly designed thermal bubble actuator and explain its working principle. Fig. 1a shows the three-dimensional drawing of the bubble-driven pulse pressure generator module and its application for the mixing enhancement in a Y-shaped microchannel, Fig. 1b is the photo of the device. The bubble-driven actuator consists of the connection channel (3) to form a loop, a bubble filter, gold film for two electrodes (4), a platinum film heater (5), and a circular chamber (6). The microheater (5) is within the diverging section of the substrate and was deposited at the back surface of the Pyrex glass cover. There are two signal wire bonding holes in the chip substrate for the electric connection with external pulse voltage generator. The two holes are sealed by glue in the system packaging. Different from other studies in the literature [11], the thin film heater has a large length to width ratio, which is 8.33 with a length of 1500 μm and a width of 180 μm. In a pulse heating cycle, a "long" bubble will be covered on the whole thin film heater during the pulse duration stage, because the whole thin film heater has relatively "high" temperature. The planar size of the bubble is comparable to the heater size. However, during the pulse off stage, the thin film heater sharply decreases its temperature, but the center part of the heater has "higher" temperature than the two side parts of the heater. Due to the well-known Marangoni effect, the initially formed "long" bubble quickly shrinks to a sphere or a circular bubble (depending on the channel depth and bubble volume), populated on the center part of the heater. During the transition from the "long" bubble to a sphere or a circular bubble, the vapor–liquid interface is strongly and quickly deformed, causing a large convection heat transfer effect across the vapor–liquid interface due to the bubble interface agitation, which is helpful for the Joule heat dissipated to the surrounding liquid and material.

Another consideration is to dissipate the heat locally generated on the thin film heater by the pulse heating to the supporting material of the microfluidic chip. We note that the rectangular film heater is suspended at the top of the diverging section. In case a "large" bubble which contacts the side walls of the diverging section, the bubble will move towards the circular chamber automatically due to the unbalance of the surface tension forces between the front and the rear sides of the bubble. This effect results

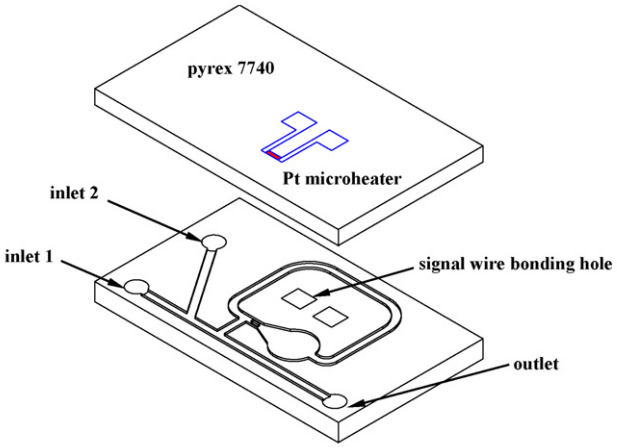

(a) three-dimensional drawing of the bubble-driven actuator for mixing enhancement

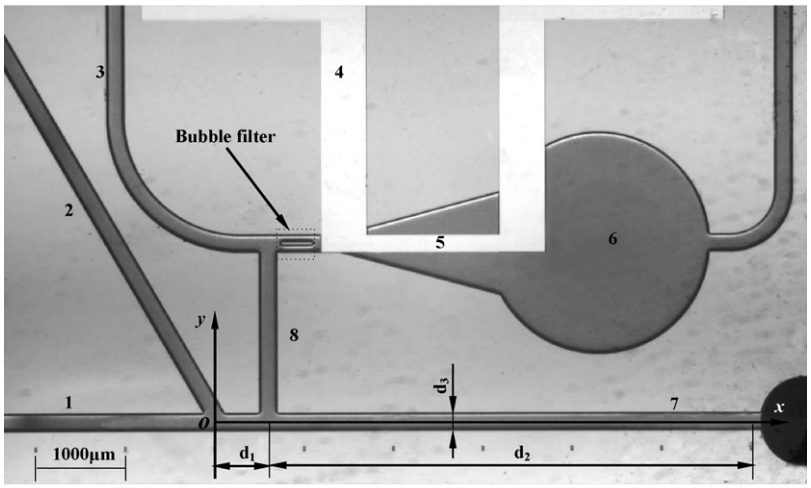

(b) photo of the microfluidic chip

Fig. 1. The design of the bubble-driven actuator for microfluidic application: (1) and (2) are the inlet fluid channels, (3) is the loop connection channel, (4) is the Au electrode, (5) is the thin film platinum film heater, (6) is the circular chamber, (7) is the mixing channel, and (8) is the pulse pressure export.

in the anticlockwise movement of the bulk fluid around the loop, and the bubble can be further condensed in the circular chamber. The fluid circulation around the loop helps to dissipate the heat to the supporting material. In such a way the temperature of the thin film heater cannot be continuously raised. The bubble filter arranged at the tail of the diverging section further protects a thermal bubble moving back and entering the pulse pressure export. The above design concept has the following characteristics:

- Pulse pressure can be generated for actuation effect.
- The thin film heater is well protected, thus it can be operated over a wide range of pulse heating parameters.
- The main microfluidic system never contacts the "high" temperature fluid and there is no bubble in the main system at all.
- The loop actuator has no moving parts thus it has high reliability. The driving source is an external low DC pulse voltage generator.
- The bubble-driven actuator can be used as a common module and integrated with any microfluidic component.

We further demonstrate the thermal bubble-driven actuator integrated with a Y-shaped microchannel for the mixing enhancement. As shown in Fig. 1, two fluid samples to be mixed enter the system from inlet ports (1) and (2) as a Y-shaped configuration. The pulse pressure output export (8) is perpendicular to the mixing channel. A planar coordinator system (x–y plane) was established, with the original point "O" located at the mixing junction, the x-axis referring to the axial flow direction and the y-axis referring to the channel width direction. The pulse pressure export is located $d_1 = 550\,\mu m$ downstream of the mixing junction. The distance between the pulse pressure export and the outlet of the fluid sample is $d_2 = 5450\,\mu m$. The mixing channel width is 200 μm and the depth is 50 μm.

2.2. Fabrication of the microfluidic chip

Fig. 2 shows the fabrication process. The etched components on the silicon wafer, including the chamber, the nozzle, the channels and the inlet/out ports, are fabricated by a two-depth ICP (inductively coupled plasma) etching process. The depth is 50 μm for all the components except that the inlet/out ports penetrated the whole substrate. Before the ICP etching, a protective silicon dioxide layer of 1 μm thick was thermally grown on the top side of the silicon wafer, acting as the mask for the 50 μm deep silicon etching. Then, a photoresist layer of 10 μm thick is spun on and patterned by photolithography, acting as the mask for the wafer etching process. After the first ICP etching process (through wafer etching), the photoresist is removed and the silicon dioxide is used as the mask to define the fluidic components. When all these steps are finished, the silicon wafer is dipped into hydrofluoric acid (HF) to remove silicon dioxide for bonding.

The microheater used to generate thermal bubbles is fabricated on the Pyrex glass, exactly facing the nozzle on the silicon wafer.

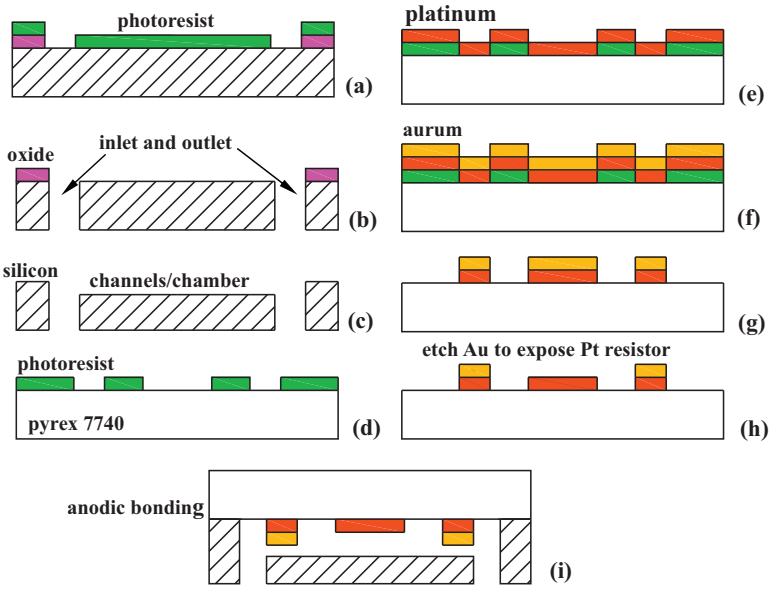

Fig. 2. The fabrication process.

The photoresist is spun on the glass and then is patterned by photolithography to define the metal structures. Three metal layers, which are 100 nm thick Ti used as adhesion layer, 200 nm thick Pt used as the microheater and 300 nm thick Au used as the contact pad, are successively sputtered on the patterned Pyrex glass. After the deposit, the metal lift-off is followed to form the metal structures. Continuing with another photolithography process to define the microheater, the Au on the top of the Pt microheater is removed by etching. It should be noted that a slot of 2 μm deep on the silicon wafer should also be fabricated by RIE before the two-depth ICP etching. This 2 μm deep slot is used to hold the protruding metal structures on the top glass, ensuring the flatting interfaces for anodic bonding.

2.3. Experimental setup and data reduction

Fig. 3a shows the microfluidic chip packaging and Fig. 3b is the experimental setup. A Harvard twin syringe pump (model 33) supplies the fluid samples for the flow system. One fluid sample is the colorless methanol, and the other sample is the black-dyed methanol. The flow rates of the two fluid samples are exactly same, which can be adjusted manually. Each component of the flow system was connected by the capillary tube with the inside diameter of 1.0 mm. A liquid collection beaker collects the mixed methanol from the outlet of the microfluidic chip. The flow Reynolds number is defined as $Re = ud/\nu$, where u is the flow velocity of the two fluid sample in the mixing channel, d is the hydraulic diameter of the mixing channel, and ν is the viscosity of the fluid methanol at the room temperature. Even though the heat flux on the microheater is high during the pulse duration stage, the microfluidic chip has room temperature, measured by a high resolution IR image system.

As shown in Fig. 3b, an EE1641 C pulse voltage generator (5) was used to generate the rectangular pulse voltage that was applied to the thin film microheater, having the output frequencies form 0.2 Hz to 20 MHz, and the output voltage amplitude from 0 to 20 V. A precision resistance box (6) provides a selective, precision external resistance that was connected with the microheater. Because the resistance is known, the current that is flowing through the microheater circuit can be obtained by measuring the voltage across the resistance. The DL 750 high speed data acquisition system (4) measures V_1 and V_2 (see Fig. 3b). The data reduction process of the pulse

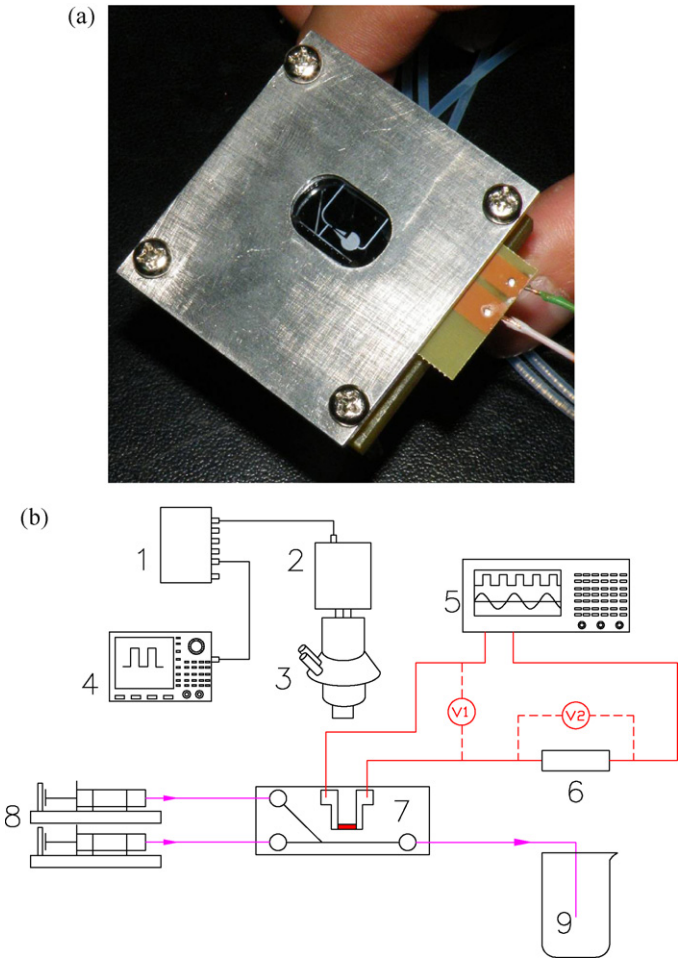

Fig. 3. Experimental setup, (a) photo of the microfluidic chip packaging, (b) experimental setup, (1) is the synchronization hub, (2) is the high speed visualization system, (3) is the microscope, (4) is the data acquisition system, (5) is the pulse voltage generator, (6) is the precision resistance box, (7) is the microfluidic chip, (8) is the twin syringe pump, and (9) is the sample collection beaker.

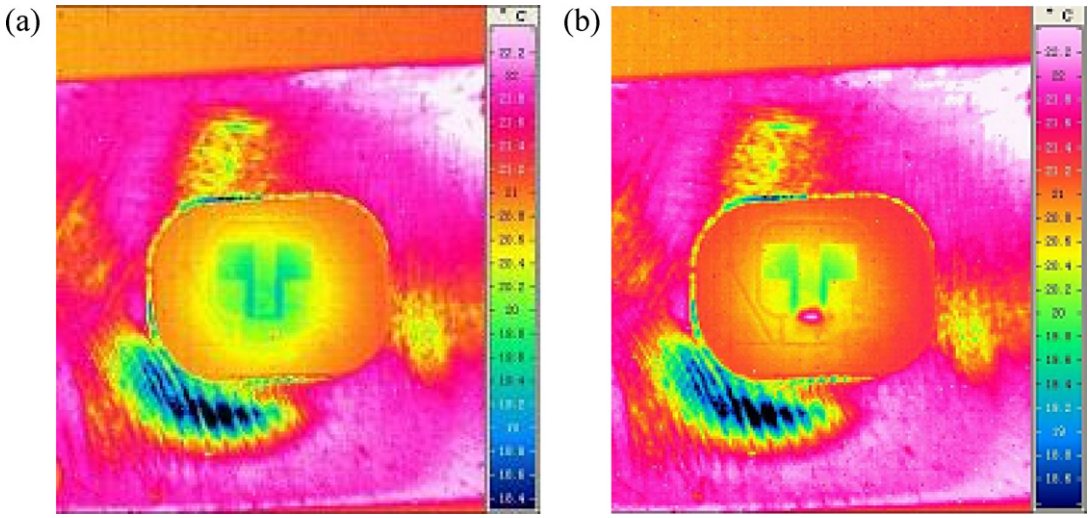

Fig. 4. IR image files showing small temperature rise of the chip surface during the operation of the microheater (a: the heater was turned off; b: the pulse voltage is applied on the heater).

heating is similar to that of Xu and Zhang [10]. The transient platinum film microheater resistance (not including the two side gold film pads, see Fig. 1b) is

$$R_{Pt} = \frac{V_1(t)R_s}{V_2(t)} - R_{Au1} - R_{Au2} \quad (1)$$

where R_s is the known precision resistance, R_{Au1} and R_{Au2} are the two gold film resistances for the wire connection (see Fig. 1a). A calibration process gives the relationship between the platinum film temperature and its resistance as $T = 63.69R_{Pt} - 644.4$. The instantaneous heating power on the platinum heater is

$$Q(t) = \left(\frac{V_2(t)}{R_s^2}\right)^2 \left(\frac{V_1(t)}{V_2(t)}R_s - R_{Au1} - R_{Au2}\right) \quad (2)$$

The heat flux on the platinum heater is computed as $q(t) = Q(t)/(LW)$, where L is the length and W is the width of the heater, they are 1500 μm and 180 μm, respectively.

It is important to estimate the temperature rise of the fluid sample in the mixing channel. In order to do so, it is necessary to estimate the average heating power generated on the microheater: $Q_{ave} = q_{ave}LW\tau_d/\tau$, where q_{ave} is the average heat flux during the pulse duration stage, τ_d is the pulse duration time and τ is the pulse cycle period. For a typical case, $q_{ave} = 30\,MW/m^2$, $L = 1500\,\mu m$, $W = 180\,\mu m$, $\tau_d = 0.5\,ms$ and $\tau = 100\,ms$, the time averaged heating power (Q_{ave}) is 40 mW. Two mechanisms dissipate the heating power: the first is to yield the temperature rise over the whole chip surface to dissipate part of the heat to the environment directly, and the second is to have a temperature rise across the inlet and out of the fluid sample: $Q_{ave} = \alpha A\,\Delta T_1 + mC_{pf}\,\Delta T_2$, where α is the natural convection heat transfer coefficient, A is the bulk chip surface area including the packaged supporting structure, ΔT_1 is the temperature rise of the bulk chip surface, m is the mass flow rate of the fluid sample in the mixing channel, C_{pf} is the specific heat of the fluid sample, and ΔT_2 is the temperature rise across the inlet and outlet of the fluid sample. A reasonable estimate of α is $10\,W/m^2\,K$ in the air environment. Giving the surface area A of 7 cm × 7 cm, the bulk chip temperature rise ΔT_1 of 0.8 °C is enough to dissipate all the heating power of Q_{ave}. Thus the temperature rise of the fluid sample in the mixing channel is neglectable. The local and temporary temperature rise of the microheater does not cause the temperature rises of the bulk chip and fluid sample in the mixing channel. Fig. 4 shows two IR image pictures on the back surface of the silicon chip for comparison, with Fig. 4a for the temperature file when the pulse voltage is turned off, and Fig. 4b for the temperature file with the pulse voltage applied on the microheater. The IR image measurement involves an uncertainty of 0.5 °C. It is seen that the two temperature files are nearly identical with the temperature uncertainty of 0.5 °C, indicating small temperature rise (less than 1 °C) of the bulk chip surface with the operation of the microheater actuator.

We use an optical system to visualize and characterize the bubble dynamics in the loop actuator and the mixing performance in the mixing channel. The optical system consists of a microscope (Leica MZ16, Germany) and a high speed visualization system (HG 100 K, USA). The system is quite sensitive to the black–white image. Different from other studies for the mixing experiment in the literature, the present study gave the spatiotemporal mixing performance in the mixing channel with millisecond time scale. During the experiment, a synchronization hub synchronizes the high speed data acquisition system and the high speed visualization system, linking the pulse heating parameters and the bubble dynamics. A central computer collects all the image files and voltage signals.

It is important to quantify the mixing degree in the mixing channel. For a fixed Reynolds number of methanol in the mixing channel (Re) and pulse heating parameters (voltage amplitude, pulse duration time, and pulse frequency), we record the consecutive image files. The Leica Qwin Image Processing and Analysis software analyzes the images at different time steps. The grayscale values are 255 for the colorless methanol and 0 for the black-dyed methanol, respectively. When the mixing process takes place, the grayscale values are in the range of 0–255. A specific pixel corresponds to a grayscale value. Similar to the previous studies [12], the mixing degree is expressed as

$$I = 1 - \frac{1}{C_v}\sqrt{\frac{\sum (C_i - C_v)^2}{N}} \quad (3)$$

where C_v is the average grayscale in a selected area, C_i is the local grayscale at the pixel i and N is the number of pixels in the selected area. The mixing degree value of 0 means no mixing occurring at all, 1 means a complete mixing. Theoretically the mixing degree are dependent on the x and y coordinates and time t, i.e., $I = I(x, y, t)$. Here we are interested in two kinds of mixing degree: (1) the transient mixing degree versus axial coordinate, i.e., $I = I(x, t)$, refers to the dynamic mixing degree along the flow direction but integrated over the whole mixing channel width.

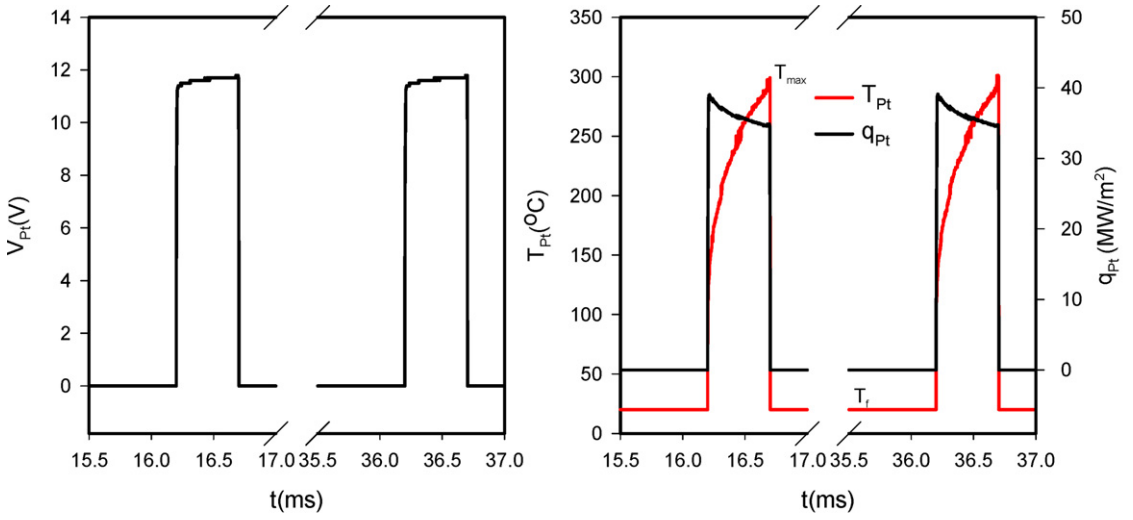

(a) voltage, temperature, and heat flux on the platinum film microheater

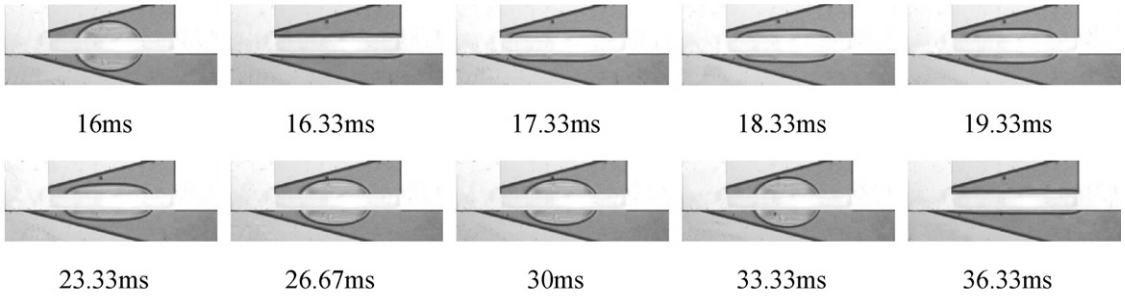

(b) bubble behavior during a full pulse cycle

Fig. 5. The pulse heating parameters on the thin film heater and bubble dynamics for a full pulse cycle (τ = 20 ms, τ_d = 0.5 ms, f = 50 Hz, noting that the time delay from T_{max} to T_f during the early pulse off stage is about 0.3–0.4 ms in Fig. 5a).

(2) The other is the time averaged mixing degree along the flow direction, i.e., $I = I(x) = (1/\tau)\int_0^\tau I(x,t)\,dt$, where τ is the pulse cycle period.

3. Results and discussion

3.1. Bubble dynamics related to the pulse heating

Before the formal experiment, the loop actuator should be vacuumed to remove the non-condensable gas and charged with liquid (methanol in this paper). The vacuum process is similar to that of a heat pipe device [13]. Non-condensable gas in the loop actuator has damping effect and weaken the pulse pressure output. Fig. 5 shows the pulse voltage, heat flux, and temperatures on the slim platinum microheater, with the pulse cycle period of 20 ms (the pulse frequency is 50 Hz). The pulse duration time is 0.5 ms. During the pulse duration stage, the voltage is about 11.5 V and slightly increased (see Fig. 5a). The temperatures are increased to about 300 °C, maximally. Heat fluxes are slightly decreased and in the range of 39–25 MW/m^2. These changes are due to the varied platinum film resistance versus temperatures. It is noted that the microheater temperatures cannot be obtained during the pulse off stage because there is no information of the heater resistance during such stage. Here we give a rough estimation of the microheater temperatures versus time following the end of the pulse duration stage. For the microheater, the mass is m_s and the specific heat is C_{ps}. Following the start of the pulse off stage, the slim microheater has thermal insulation boundary condition at the bonding surface with the glass cover, but it has the convection heat transfer boundary condition with the exposed fluid sample. The following equation gives the temperature response during the pulse off stage:

$$m_s C_{ps}\frac{dT}{dt} = -\alpha_e LW(T - T_f) \quad (4)$$

where α_e is the convection heat transfer coefficient between the heater surface and the fluid sample in the diverging section, T is the heater temperature, and T_f is the fluid temperature. The temperature at the start of the pulse off stage is T_{max}. Let $K = \alpha_e LW/(m_s C_{ps}) = \alpha_e/(\rho_s C_{ps}\delta)$, where ρ_s is the platinum density, δ is the platinum film thickness, which is 200 nm in this study. Eq. (4) has the following solution:

$$T = (T_{max} - T_f)\, e^{-Kt} + T_f \quad (5)$$

The ultra-thin microheater yields a very large K value. The larger the K value, the faster the microheater temperatures drop. For example, giving ρ_s = 21.4 g/cm^3 and δ = 200 nm for platinum film, and assuming α_e of 10^4 W/m^2 K, the estimated K reaches 17,310 s^{-1}. Based on Eq. (5), the microheater temperatures can drop from 300 °C to 21.5 °C in 0.3 ms after the pulse voltage is receded, assuming T_f of 20 °C.

Fig. 5b gave the bubble image for a set of specific time. At the end of a previous cycle such as at t = 16 ms, the bubble is elliptical and located at the center part of the slim heater. At that time the slim heater has low temperature but the center part of the slim heater has slightly higher temperature than the front and rear sides. The Marangoni effect causes the bubble populated their. Once the pulse voltage is applied on the heater during the pulse duration stage, the bubble is quickly deformed and covered on the whole slim heater, as shown in the image at t = 16.33 ms. The images from the time of

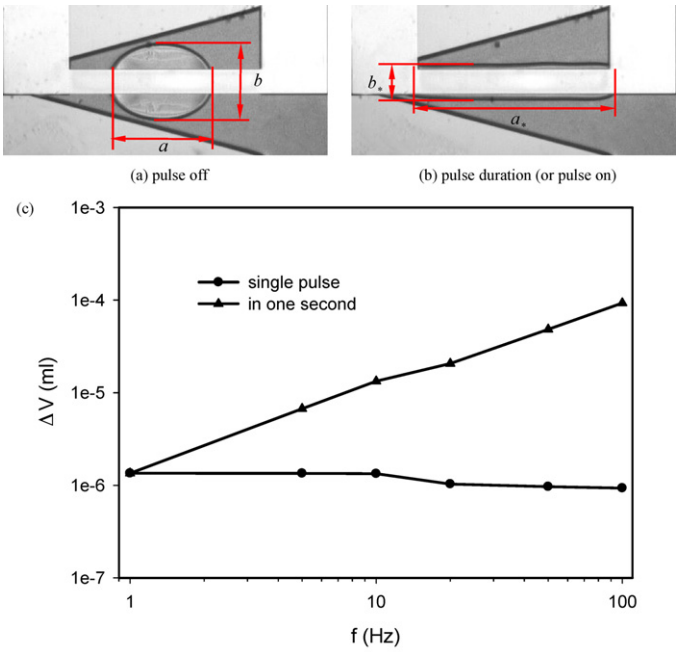

Fig. 6. The stroke volume and "second stroke volume" for the bubble-driven actuator.

17.33 ms to 33.33 ms show the transition from a slim bubble to an elliptical one when the voltage is receded from the heater.

During a complete cycle, the liquid volume pumped out of the loop actuator is exactly equal to that sucked into the loop. The working principle of the thermal bubble-driven actuator is similar to human being's heart. We define the volume change ΔV during the bubble expansion-shrinkage process in one cycle, which is called the stroke volume. Fig. 6a and b shows the bubble on the platinum film heater at the pulse off stage and pulse duration stage. Considering the shallow channel, we assume that the bubble could fill the whole channel depth. The stroke volume in one pulse cycle is computed as

$$\Delta V = a_* b_* \delta - \frac{1}{4}\pi a b \delta \tag{6}$$

where δ is the channel depth, definition of other parameters in Eq. (6) can be seen in Fig. 6.

Another important parameter is the stroke volume in 1 s, we call it as the "second stroke volume" (ΔV_S), which is important for the pulse pressure export for microfluidic applications. It is easy to have the express of $\Delta V_S = \Delta V \cdot f$, here f is the pulse frequency. Fig. 6c shows that the stroke volume is about 1×10^{-6} ml. On the other hand, the "second stroke volume" is nearly increased linearly versus pulse frequency, reaching about 1×10^{-4} ml at the pulse frequency of 100 Hz.

In order to observe the oscillation flow in the pulse pressure export directly, we inject a tiny gas bubble in the pulse pressure export channel on purpose, acting as the tracing bubble there, not-

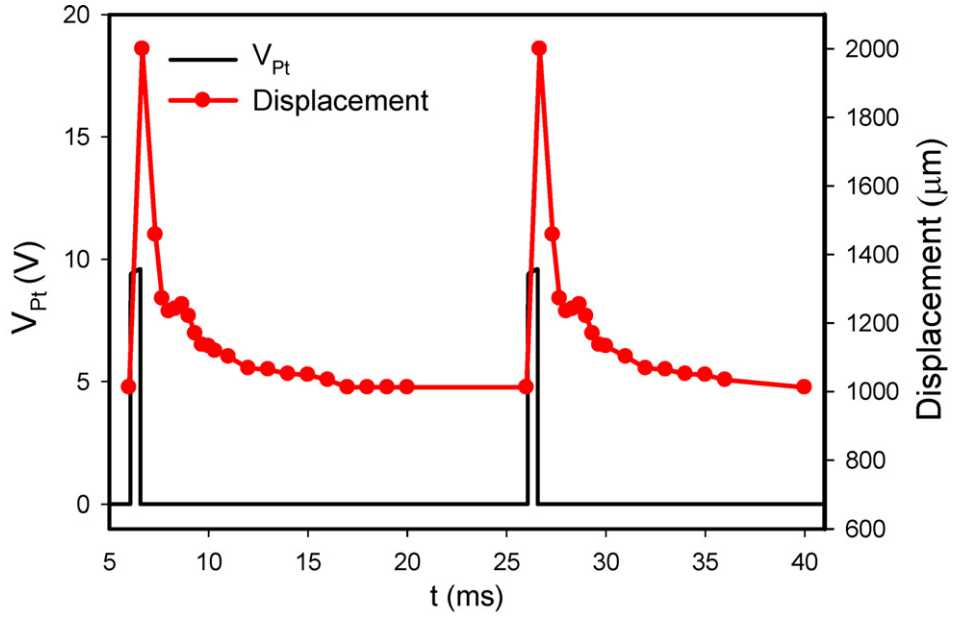

(a) voltage on the microheater and the tracing bubble displacement in the pulse pressure export channel

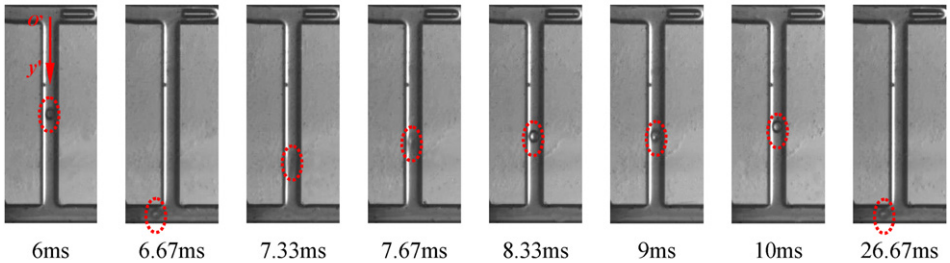

(b) oscillation movement of the tracing bubble in the pulse pressure export channel

Fig. 7. Oscillation movement of the tracing bubble in the pulse pressure export channel at f = 50 Hz.

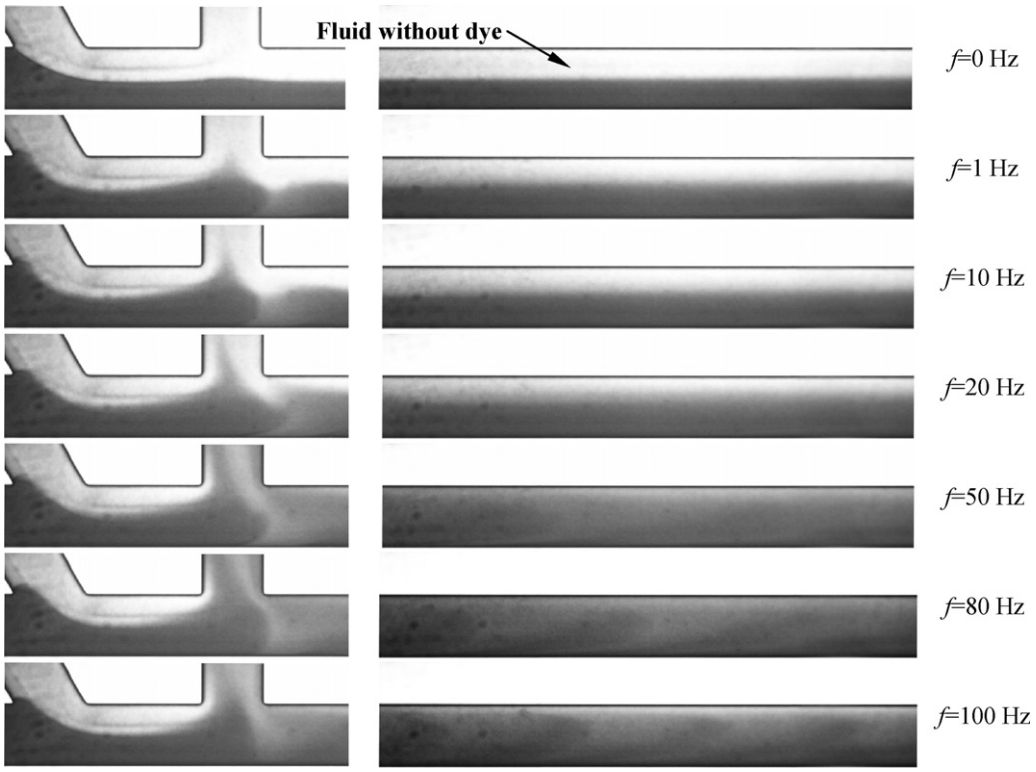

Fig. 8. Effect of pulse heating frequency on the mixing patterns in the mixing channel for $Re = 1$ (for each frequency, images are shown for the upstream and downstream of the mixing channel).

ing that such a bubble is not the thermal bubble generated by the pulse heating on the platinum heater. Fig. 7a illustrates the pulse voltage on the microheater and the tracing bubble displacement versus time. We temporarily set a coordinate $o'y'$ with o' located at the tip of the loop channel, and y' as the flow direction of the pulse pressure export channel (see Fig. 7b). Because the pulse duration time is short and the temporary heat flux on the microheater is significantly high, the tracing bubble has a sharp increase of the displacement versus time once the voltage is applied on the microheater, indicating a great acceleration of the tracing bubble. The tracing bubble was initially located at the center of the pulse pressure export channel at $t = 6.0$ ms, but was pushed to the mixing channel at $t = 6.67$ ms (see Fig. 7b). After the pulse duration stage is over, the tracing bubble was quickly sucked into the pulse pressure export channel, followed by a slow change of the tracing bubble displacement. The thermal bubble interface is strongly deformed, causing an enhanced condensation heat transfer between the thermal bubble and the surrounding liquid. The oscillation flow of the fluid in the pulse pressure export channel is similar to the piston movement in a cylinder.

3.2. Mixing patterns in the mixing channel

Now we examine the mixing performance enhanced by the pulse pressure. Fig. 8 shows the mixing patterns for different pulse frequencies. Generally there are two mixing patterns. The first type, called the wavy interface pattern, appears without pulse pressure ($f = 0$) and with pulse frequencies of 1 Hz and 10 Hz (see Fig. 8). The mixing between the two fluid samples (one is the colorless methanol and the other is the black-dyed methanol) are not well mixed thoroughly, a wavy mixing interface exists along the flow direction, except that the mixing interface is not deformed at all for the no pulse pressure run ($f = 0$), under which the molecular diffusion domains the process. However, for the pulse frequencies larger than 20 Hz, the wavy mixing interface disappears. Instead, there are a set of mixing clouds populated along the flow direction. We call this type of mixing as the cloud mixing pattern, which can enhances the mass transfer between the two fluid samples.

We further examine the two types of mixing patterns dynamically for a set of time steps. We present the transient evolution of the wavy interface pattern for $f = 10$ Hz in Fig. 9. A complete pulse cycle is focused. A clear and relatively straight interface appears at the end of a previous pulse cycle (see the image at $t = 48$ ms in Fig. 9). When the voltage is applied on the microheater for a new pulse cycle, the thermal bubble expansion on the microheater exports the fluid to the mixing channel, forming a wavy interface, consisting of a valley and a massif. During the pulse off stage, the wavy interface is traveling downstream of the mixing channel. The fluid is sucked from the mixing channel to the pulse pressure export channel due to the shrinkage of the thermal bubble on the microheater (see the images for $52 \text{ ms} < t < 62$ ms in Fig. 9). The beginning of a new cycle (see the image at $t = 149$ ms in Fig. 9) exactly repeats the state at $t = 49$ ms. Generally the wavy interface for the low pulse frequency run is due to the fluid discharging from the pulse pressure export channel can not thoroughly penetrate the whole mixing channel width.

Comparatively, Fig. 10 illustrates the transient evolution of the cloud mixing pattern for the pulse frequency of 100 Hz. During the pulse duration stage, the fluid coming from the pulse pressure export thoroughly penetrates the whole mixing channel width. Because the pulse duration stage is so short that we only have one image for such state (see the image at $t = 5$ ms in Fig. 10). During the pulse off stage, the fluid in the mixing channel can be sucked into the pulse pressure export channel. The expansion and shrinkage of the thermal bubble on the microheater in one pulse cycle forms a mixing cloud in the mixing channel.

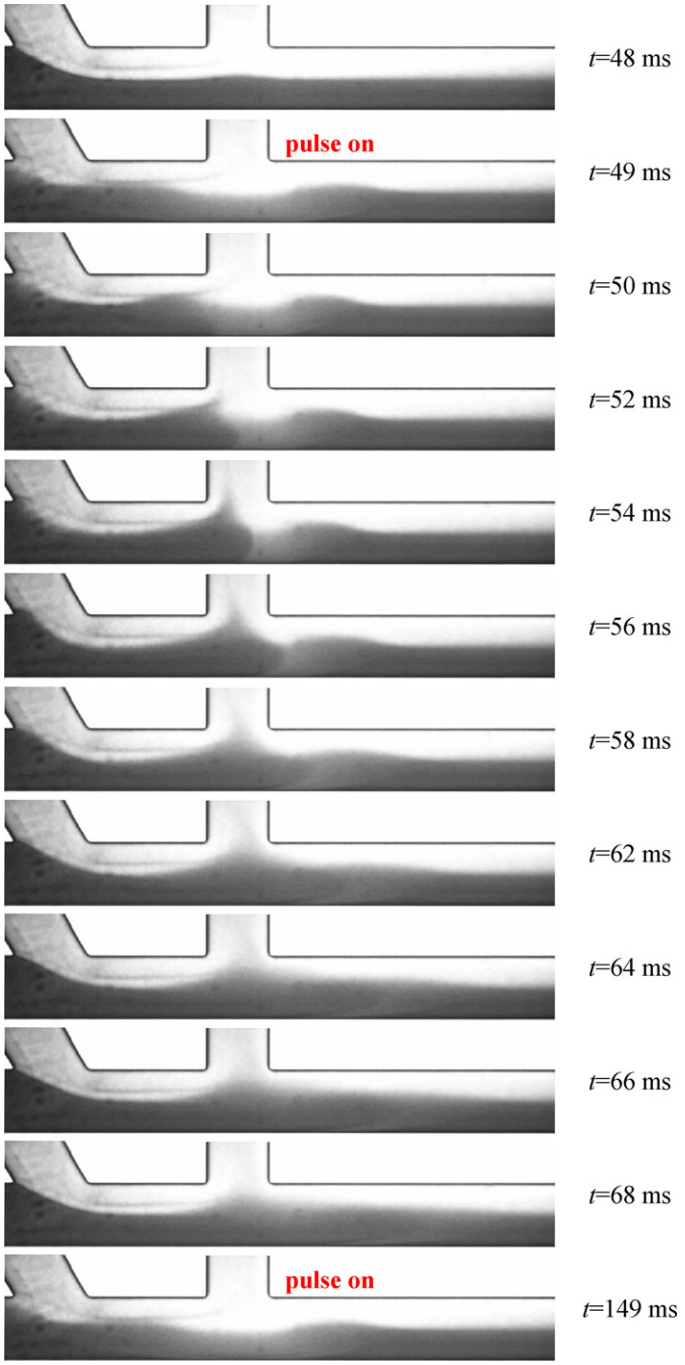

Fig. 9. Transient wavy interface mixing pattern in one full pulse cycle for low pulse frequency of 10 Hz.

3.3. Characterization of the mixing performance

Fig. 11 shows the transient mixing degrees at the location of $x = 1000\ \mu m$ for the Reynolds number of 1. The mixing degrees are increased with increases of the pulse frequencies, i.e., they are highest for the pulse frequency of 100 Hz, and lowest for the pulse frequency of 10 Hz. Meanwhile, they are varied in the ranges of 0.104–0.163, 0.743–0.807, and 0.846–0.859 for the pulse frequencies of 10 Hz, 50 Hz, and 100 Hz, respectively. The locally mixing degrees are varied periodically against the time. The cycle period of the transient mixing degree is exactly the same as that of the pulse heating applied on the microheater, further indication the pulse pressure effect by the expansion-shrinkage of the thermal bubble on the microheater.

We examine the variation of the grayscale values in the mixing channel width direction in Fig. 12. It is seen that the grayscale values without pulse pressure effect ($f = 0$) and with the low pulse frequency of 10 Hz have significant non-uniform distribution against the centerline of the mixing channel, indicating half channel is occupied by the colorless methanol and the other part is occupied by the black-dyed methanol. Mixing performance is poor at such low pulse frequencies, which is due to the low "second stroke volume". The non-uniformity of the grayscale values is significantly improved at high pulse frequencies of 50 Hz and 100 Hz. The grayscale values are almost uniform across the whole channel width for the pulse frequency of 100 Hz.

Now we study the mixing performance along the flow direction. Fig. 13a shows that the grayscale values are oscillating periodically

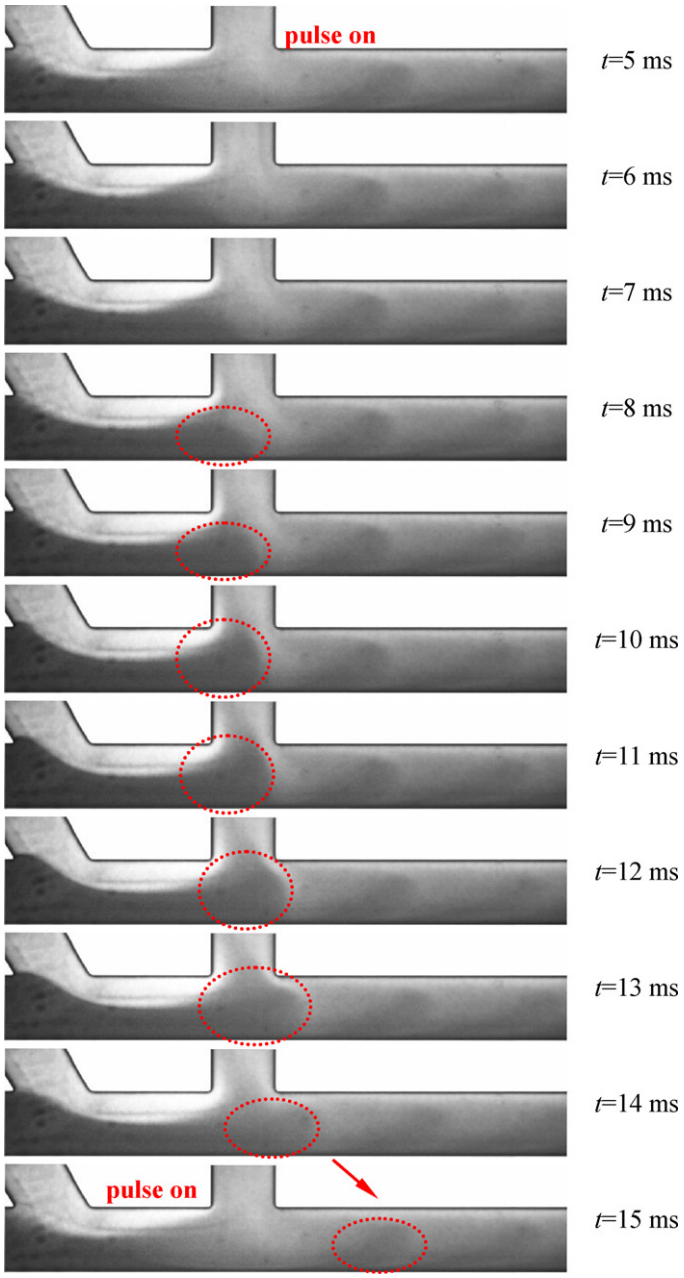

Fig. 10. The transient cloud mixing pattern in one full pulse cycle for high pulse heating frequency of 100 Hz.

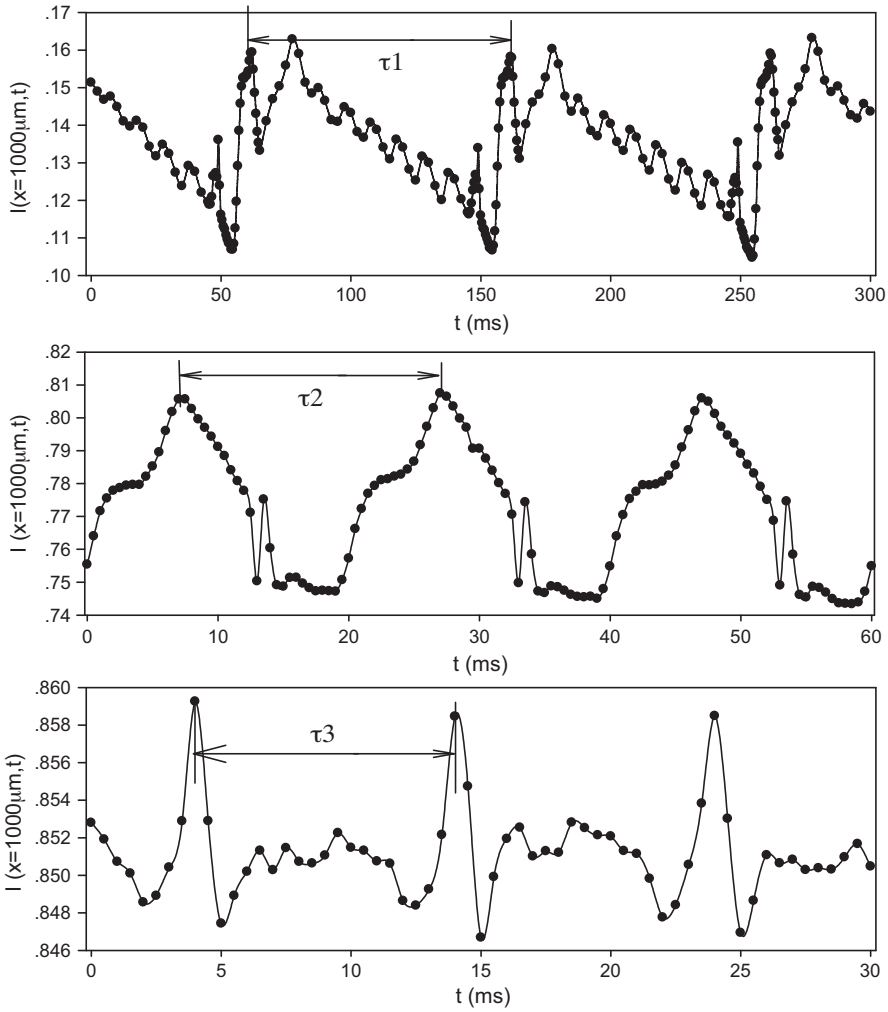

Fig. 11. The transient mixing degree at $x = 1000$ μm for $Re = 1$ (effect of pulse heating frequencies, (a) for $f = 10$ Hz, (b) for $f = 50$ Hz, and (c) for $f = 100$ Hz).

along the flow direction. The oscillation amplitudes are decreased with increases of the x-coordinate. It is noted that the grayscale value curves shown in Fig. 13a is for a specific time. The curves shall be changed with time evolution, but the curve shapes are similar. The oscillation is weak for $x > 1500$ μm, indicating a quasi-uniform distribution of the fluid sample concentrations following about 1 mm downstream of the pulse pressure export. We study the time averaged mixing degrees versus the x-coordinate in Fig. 13b. The mixing degrees are low and about 0.1 for the pulse frequency of 10 Hz, but they are much higher for the pulse frequencies of 50 Hz and 100 Hz. Seeing from Fig. 13b is that the mixing degrees are sharply increased with the x-coordinate in the range of 0–1 mm, noting that the pulse pressure export is located at $x = 545$ μm. They have slight increase with the x-coordinate beyond 1 mm. The mixing process is nearly complete in a couple of millimeter following the pulse pressure export. The mixing length is defined as the distance between the local position and the pulse pressure export, which is a couple of millimeter for the present design. The mixing degree can reach 0.94 for the pulse frequency of 100 Hz.

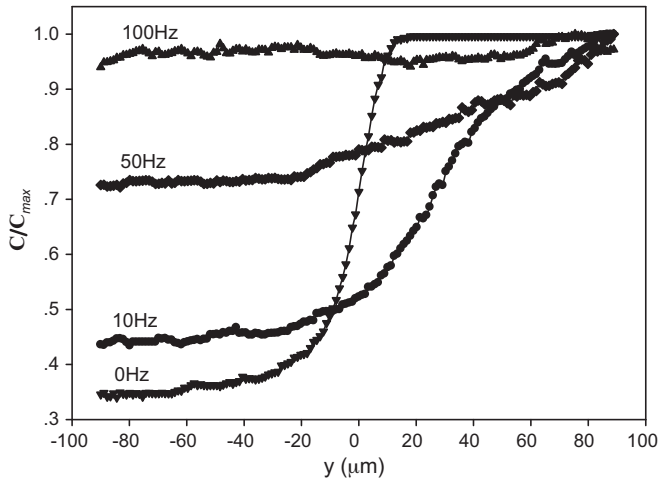

Fig. 12. Normalized grayscale value across the mixing channel width at $x = 4000$ μm at the four pulse heating frequencies.

Finally, effect of the Reynolds numbers on the mixing performance is given in Fig. 14. It is found that the time averaged mixing degrees at the location of $x = 4000$ μm are almost independent of the Reynolds number. This is true for other locations. The finding is also consistent with other studies reported in the literature [1,14].

This is a primary study using the novel bubble-driven actuator to enhance mixing performance in microchannels. The working fluid is methanol, which is toxic for human being's organism and is not suitable to be used as liquid carrier in a microfluidic device. However, the proposed microfluidic device can work well with other bio-fluid samples theoretically. Future studies will try other carrier fluid and further demonstrate the advantageous of the proposed bubble-driven actuator.

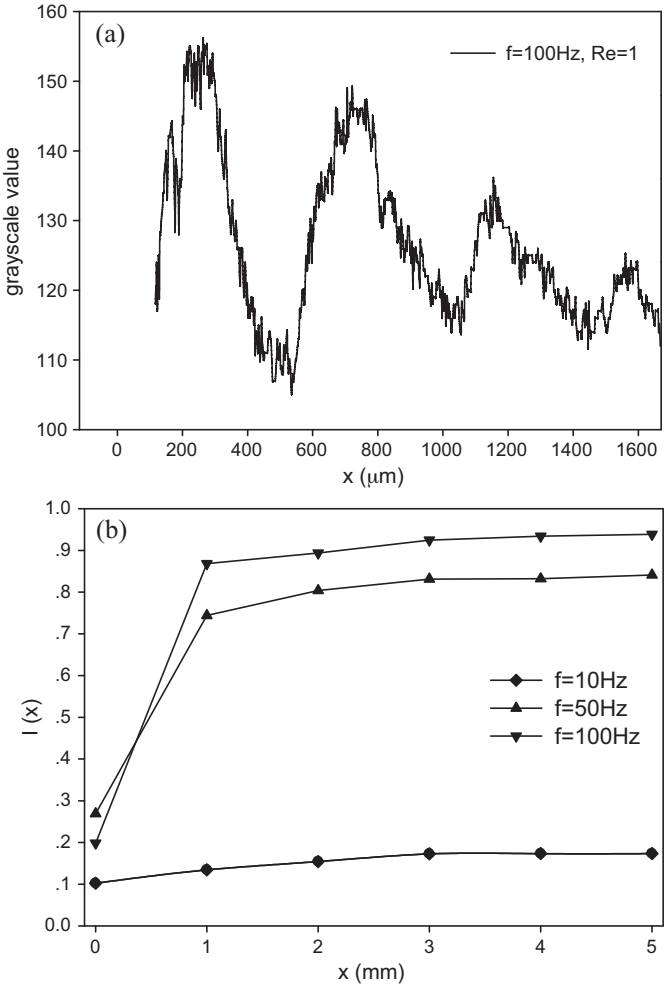

Fig. 13. The time averaged mixing degree along the flow direction for the three pulse heating frequencies.

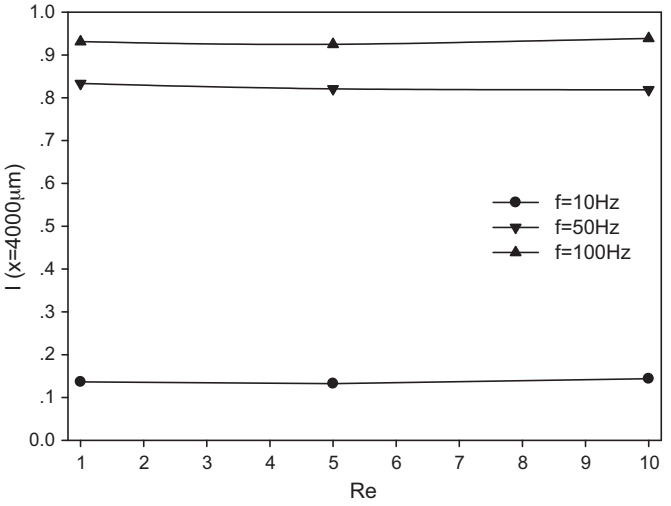

Fig. 14. The mixing degree independent of the Reynolds number at $x = 4000\ \mu m$.

4. Conclusions

We demonstrate a thermal bubble-driven loop actuator for microfluidic applications. The configuration consists of a diverging section and a circular chamber. A slim microheater with large length to width ratio was deposited on the back surface of the glass cover, facing the diverging section of the bottom substrate. The transition from a "long" bubble during the pulse duration stage to a sphere or a circular bubble during the pulse off stage exports the pulse pressure and causes a large convection heat transfer at the vapor–liquid interface, which is helpful to protect the microheater from burnout. The loop configuration pumps the bulk fluid movement around the loop, dissipating the locally Joule heat generated by the pulse heating to the supporting structure of the microfluidic chip, keeping the microfluidic chip at the room temperature level.

The loop actuator is suitable for microfluidic applications in which pulse pressure is needed, featuring the following advantages: (1) the thin film microheater is well protected, thus it can be operated over a wide range of pulse heating parameters. (2) The main microfluidic system never contacts the "high" temperature fluid and there is no bubble in the main system at all. (3) The loop actuator has no moving parts thus it has high reliability. The driving source is a low DC pulse voltage generator.

We demonstrate the loop actuator used for mixing enhancement. The findings are as follows: (1) the low pulse frequency such as 10 Hz yields a wavy mixing interface in the mixing channel, but the discharged fluid from the pulse pressure export thoroughly penetrates the whole mixing channel width at high pulse frequencies, resulting in a set of mixing clouds in the mixing channel. (2) The mixing degrees are increased with increases of pulse frequencies. (3) The fluid samples are uniformly distributed across the channel width direction for the pulse frequency of 100 Hz. (4) The cycle periods of the transient mixing degrees are exactly equal to the pulse heating cycle periods. (5) The mixing degree can reach 0.94 for a short mixing length of a couple of millimeter for the pulse frequency of 100 Hz. (6) The mixing degrees are independent of the Reynolds number in the mixing channel.

Acknowledgements

This work is supported by the National Natural Science Foundation of China (Nos. 50825603 and U1034004), and the Basic Research Program (973 program) with the contract number of 2011CB710703.

References

[1] A.D. Stroock, S.K.W. Dertinger, A. Ajdari, I. Mezic, H.A. Stone, G.M. Whitesides, Chaotic mixer for microchannels, Science 295 (2002) 647–651.
[2] K.F. Lei, W.J. Li, A novel in-plane microfluidic mixer using vortex pumps for fluidic discretization, J. Assoc. Lab. Autom. 13 (2008) 227–236.
[3] Y. Zhen, S. Matsumoto, H. Goto, M.M. Matsumoto, R. Maeda, Ultrasonic micromixer for microfluidic systems, Sens. Actuators A: Phys. 93 (2001) 266–272.
[4] L.H. Lu, K.S. Ryu, C. Liu, A magnetic microstirrer and array for microfluidic mixing, J. Microelectromech. Syst. 11 (2002) 462–469.
[5] R.H. Liu, J. Yang, M.Z. Pindera, M. Athavale, P. Grodzinski, Bubble-induced acoustic micromixing, Lab on Chip 2 (2002) 151–157.
[6] I. Glasgow, N. Aubry, Enhancement of microfluidic mixing using time pulsing, Lab on Chip 3 (2003) 114–120.
[7] M.Z. Huang, R.J. Yang, C.H. Tai, C.H. Tsai, L.M. Fu, Application of electrokinetic instability flow for enhanced micromixing in cross-shaped microchannel, Biomed. Microdevices 8 (2006) 309–315.
[8] P. Tabeling, M. Chabert, A. Dodge, C. Jullien, F. Okkels, Chaotic mixing in cross-channel micromixers, Philos. Trans. R. Soc. Lond. A 362 (2004) 987–1000.
[9] J.H. Tsai, L.W. Lin, Active microfluidic mixer and gas bubble filter driven by thermal bubble micropump, Sens. Actuators A: Phys. 97–98 (2002) 665–671.
[10] J. Xu, W. Zhang, Effect of pulse heating parameters on the microscale bubble dynamics at a microheater surface, Int. J. Heat Mass Transfer 51 (2008) 389–396.
[11] J. Xu, G. Liu, W. Zhang, Q. Li, B. Wang, Seed bubbles stabilize flow and heat transfer in parallel microchannels, Int. J. Multiphase Flow 35 (2009) 773–790.
[12] Y.K. Lee, P. Tabeling, C. Shih, C.M. Ho, Characterization of a MEMS-fabricated mixing device, in: ASME International Mechanical Engineering Congress & Exposition, Orlando, FL, 2000, pp. 505–511.
[13] J.L. Xu, Y.X. Li, T.N. Wong, High speed flow visualization of a closed loop pulsating heat pipe, Int. J. Heat Mass Transfer 48 (2005) 3338–3351.
[14] Y.Z. Liu, B.J. Lim, H.J. Sung, Two-fluid mixing in a microchannel, Int. J. Heat Fluid Flow 25 (2004) 986–995.

Biographies

B. Wang is a PhD student now at the Department of Mechanical Engineering of The Hong Kong University of Science and Technology. His current research focuses in micro droplet evaporation and spreading on patterned surface combining the μPIV technology. He obtained his bachelor's degree in 2005 from Tianjin University of Science and Technology, China and master's degree in 2010 from Chinese Academy of Sciences, China under the supervision of Prof. Jinliang Xu.

J.L. Xu is a professor and the director of the Beijing Key Laboratory of New and Renewable Energy, North China Electric Power University. He received his PhD at the Department of Power and Energy Engineering, Xi'an Jiaotong University, in 1995. He joined Tsinghua University as a post-doctor from 1995 to 1997. He worked in Florida International University (USA), University of Notre Dame (USA), and Nanyang Technological University (Singapore) from 1998 to 2001. He was a Professor and the director of the academic committee of Guangzhou Institute of Energy Conversion, Chinese Academy of Sciences and setup the micro energy system laboratory, from 2002 to 2008. He received the National Natural Science Fund for Distinguished Young Scholars in 2008. His current research interests include the solar and geothermal energy utilization and power generation, micro energy system, and micro/nano scale heat transfer. He published 50 articles in referred international journals. He is a referee for 14 international journals. He presented five keynote speeches in international conferences, and served as the track, or session chair for the international conferences.

W. Zhang is an associate professor in School of Renewable Energy, North China Electric Power University since August 2009. He received his PhD in June 2008 from Chinese Academy of Sciences and then worked as a postdoctoral researcher on the topic of multiphase microreactor from July 2008 to July 2009 in Eindhoven University of Technology, the Netherlands. He has published more than 20 articles in peer-reviewed scientific journals. His research interests cover multiphase flow and heat transfer in microsystems, low grade heat recovery and heat transfer of supercritical fluids.

Y.X. Li is an associate professor in Guangzhou Institute of Energy Conversion, Chinese Academy of Sciences. She got her BS degree in Research Institute of Refrigerating and Thermal Engineering, College of Mechanical Engineering, Tongji University, China, in 2001, master degree in School of Energy Science and Engineering, Harbin Institute of Technology, China, in 2003, and PhD degree in Guangzhou Institute of Energy Conversion, Chinese Academy of Sciences, China, in 2009. Her current research interests include multiphase flow and heat transfer, numerical study of solar radiation heat transfer in complex geometries, and molecular dynamics and its hybrid simulation for microfluidics.